Published in final edited form as:
Int J Pharm. 2014 April 25; 465(0): 52–62. doi:10.1016/j.ijpharm.2014.01.043.

Development of High Efficiency Ventilation Bag Actuated Dry Powder Inhalers

Srinivas R.B. Behara[1,2], **P. Worth Longest**[1,2,*], **Dale R. Farkas**[1], and **Michael Hindle**[2]

[1]Department of Mechanical and Nuclear Engineering, Virginia Commonwealth University, Richmond, VA

[2]Department of Pharmaceutics, Virginia Commonwealth University, Richmond, VA

Abstract

New active dry powder inhaler systems were developed and tested to efficiently aerosolize a carrier-free formulation. To assess inhaler performance, a challenging case study of aerosol lung delivery during high-flow nasal cannula (HFNC) therapy was selected. The active delivery system consisted of a ventilation bag for actuating the device, the DPI containing a flow control orifice and 3D rod array, and streamlined nasal cannula with separate inlets for the aerosol and HFNC therapy gas. *In vitro* experiments were conducted to assess deposition in the device, emitted dose (ED) from the nasal cannula, and powder deaggregation. The best performing systems achieved EDs of 70–80% with fine particle fractions <5 μm of 65–85% and mass median aerodynamic diameters of 1.5 μm, which were target conditions for controlled condensational growth aerosol delivery. Decreasing the size of the flow control orifice from 3.6 to 2.3 mm reduced the flow rate through the system with manual bag actuations from an average of 35 to 15 LPM, while improving ED and aerosolization performance. The new devices can be applied to improve aerosol delivery during mechanical ventilation, nose-to-lung aerosol administration, and to assist patients that cannot reproducibly use passive DPIs.

Keywords

Active dry power inhaler (DPI); high efficiency DPI; excipient enhanced growth (EEG) formulation; noninvasive ventilation; nose to lung aerosol delivery; streamlined ventilation components

1. Introduction

Effective delivery of inhaled pharmaceutical aerosols relies on the product formulation, device design, and correct patient usage including sufficient inspiratory effort (Dolovich and

*Corresponding author: Dr. P. Worth Longest, PhD, Virginia Commonwealth University, 401 West Main Street, P.O. Box 843015, Richmond, VA 23284-3015, Phone: (804)-827-7023, Fax: (804)-827-7030, pwlongest@vcu.edu.

Dhand, 2011; Smith et al., 2010; Weers et al., 2010). Dry powder inhalers (DPIs) are currently popular aerosol delivery platforms with a number of advantages that can be broadly divided into categories based on operation by a passive or active method (Islam and Cleary, 2012; Newman and Busse, 2002). Passive devices depend on patient inspiratory effort, and in contrast, active devices reduce the dependence on the patient inspiratory effort by providing energy input from an external source to aerosolize and deliver the powder (Concessio et al., 1997; Crowder and Hickey, 2006). Because active devices are not dependent on patient inhalation rate they are useful in a number of situations such as mechanical ventilation (Tang et al., 2011), pediatric and geriatric patients with low inhalation flow rates (Laube et al., 2012), nose-to-lung aerosol delivery (Golshahi et al., 2013; Longest et al., 2011), and aerosol delivery to test animals (Grainger et al., 2004).

Dry powder inhalers provide a number of advantages for pharmaceutical aerosol delivery compared with pressurized metered dose inhalers (MDIs) and nebulizers, which include product stability (LiCalsi et al., 1999), high drug mass per inhalation (Geller et al., 2011), less susceptibility to microbial growth, and low cost (Islam and Cleary, 2012). Relatively few studies have considered the use of active DPIs for aerosol delivery compared with passive devices (Everard et al., 1996; Grainger et al., 2004; Harper et al., 2007; Pohlmann et al., 2013; Tang et al., 2011; Ungaro et al., 2006). Considering the use of active devices with mechanical ventilation systems, Everard et al. (1996) aerosolized budesonide through straight endotracheal tubes (9.0 mm internal diameter and 32 cm in length) using the Turbuhaler® DPI enclosed in an airtight casing, and reported 20% mean drug delivery through the system at an inspiratory tracheal flow rate of approximately 60 LPM. Tang et al. (2011) aerosolized mannitol powders into endotracheal and tracheostomy tubes of 7.0–9.0 mm internal diameters and 95–300 mm lengths. The powders were aerosolized into the tubes using the Osmohaler® by squeezing a standard adult ventilation bag resulting in flow rates between 111–116 LPM with particle size distribution at the end of the tubes measured using an impinger. The emitted fine particle fractions (<5 μm based on loaded dose) ranged from 20–30% and the emitted doses were in the range of 50–60%. Considering aerosol delivery to infants, Laube et al. (2012) administered radiolabeled powder through a facemask into the Sophia anatomical infant nose-throat model (SAINT) using the Solovent® active DPI. The authors reported 90% emitted dose from the Solovent device with a majority of the powder retained in the spacer, resulting in a range of approximately 0.3–4% deposition on a filter positioned distal to the SAINT model. Pohlmann et al. (2013) recently demonstrated the continuous delivery of high dose spray dried surfactants to infants and neonates receiving mechanical ventilation using an active DPI system and reported a delivery efficiency of 55% prior to the patient interface, which was envisioned to be infant nasal prongs. Based on these studies and others, active DPI devices used during mechanical ventilation or with a mask typically deliver approximately 0.3–60% of the aerosolized drug to the lungs and provide FPFs < 5 μm of approximately 20–30%.

A recent strategy to improve the performance of passive DPIs has been the development of controlled condensational growth techniques (Hindle and Longest, 2010, 2012; Longest and Hindle, 2011; Longest et al., 2009). In this approach, an aerosol is delivered to the respiratory tract with an initial submicrometer or sufficiently small size to minimize upper airway deposition. Droplet size increase through condensational growth allows for retention

of the aerosol as well as potentially targeting the location of deposition in the lungs. Techniques to produce the required size increase include enhanced condensational growth (ECG) and enhanced excipient growth (EEG). In the ECG approach, the aerosol is delivered with air saturated with water vapor a few degrees above body temperature, which creates supersaturated relative humidity (RH) conditions in the lungs to foster condensational growth of the droplets (Hindle and Longest, 2010; Tian et al., 2011). Using the ECG approach, the initial particles or droplets may be non-hygroscopic or may contain a hygroscopic excipient to further enhance the rate of aerosol growth and final droplet size. With EEG, formulated particles contain a combination of a drug and a hygroscopic excipient and the natural RH in the lungs provides the water vapor source for aerosol size increase (Hindle and Longest, 2012; Longest and Hindle, 2011). Combination particles that contain both a therapeutic agent and hygroscopic excipient in order to create aerosol size increase in the airways are referred to as an EEG formulation (Hindle and Longest, 2012; Son et al., 2013a).

Considering passive DPIs for oral inhalation using the patient's inspiratory effort, Son et al. (2013a) optimized an EEG formulation with mannitol as the hygroscopic excipient and demonstrated a reduction in mouth-throat deposition from greater than 80% of the drug with a common commercial device and formulation to less than 5% with the same device and EEG formulation. Son et al. (2013b) then considered this optimized formulation in commercial and modified DPIs. Using a new 3D rod array design to deaggregate the EEG formulation produced fine particle fractions based on emitted dose (ED) less than 5 μm ($FPF_{<5\mu m/ED}$) and less than 1 μm ($FPF_{<1\mu m/ED}$) of 97.3% and 38.8%, respectively, at a pressure drop of 4 kPa and flow rate of 45 LPM (Son et al., 2013b). The combination of the EEG formulation and 3D rod array DPI was shown to produce less than 3% mouth-throat deposition and an aerosol with an MMAD of 2.8 μm after exposure to respiratory temperature and RH conditions (Son et al., 2013b).

Longest et al. (2013b) developed the 3D rod array design used in the study of Son et al. (2013b) by considering eight different deaggregation structures using a combination of CFD and *in vitro* experiments. The 3D rod array design was found to maximize the deaggregation of the carrier free EEG formulation powders, which correlated well with a new predictive deaggregation parameter termed non-dimensional specific dissipation (NDSD) (Longest et al., 2013b). High efficiency passive DPIs for use with EEG formulations were characterized by Behara et al. (2013a) as achieving an emitted dose of ≥75%, an aerosol MMAD of ≤1.5 μm, which is expected to produce <5% mouth-throat deposition (Son et al., 2013a; Son et al., 2013b), and a $FPF_{<5\mu m/ED}$≥90%. By introducing a new capsule chamber design along with the 3D rod array flow passage (Longest et al., 2013b), Behara et al. (2013a) demonstrated further improved deaggregation of an EEG formulation. Coating of the capsule and device surfaces with low surface energy PTFE was also shown to improve emitted dose (Behara et al., 2013a). The resulting new high efficiency inhaler had an emitted dose of greater than 80% and produced an aerosol with an MMAD = 1.3 μm and $FPF_{<5\mu m/ED}$ > 90%. In a subsequent study, Behara et al. (2013b) developed a second DPI design that achieved high efficiency performance without the need for PTFE coating and that provided visual feedback of correct inhalation flowrate. Furthermore, both of these high

efficiency DPIs were shown to not be sensitive to inhalation pressures in the tested range of 2 to 4 kPa (Behara et al., 2013a; Behara et al., 2013b). A number of recent *in vitro* and CFD studies have also demonstrated that combination drug and hygroscopic excipient particles used in EEG formulations increase in size when exposed to respiratory thermodynamic conditions by an amount sufficient to provide nearly full lung retention of the aerosol (Hindle and Longest, 2012; Longest and Hindle, 2011, 2012; Tian et al., 2013; Tian et al., 2011). Based on these previous studies, the combination of EEG formulations and new devices with 3D rod arrays provide excellent performance for passive operation. However, it is currently not known if this approach can be effectively translated to an active DPI system.

Of the many applications for active DPIs, mechanical ventilation provides a highly challenging scenario for effective respiratory drug delivery (Ari and Fink, 2012; Dhand, 2012). During mechanical ventilation, the aerosolized medication is required to pass through the generation device, connective tubing, connectors (such as a tee and wye), and patient interface, all of which typically include relatively small diameters and sudden changes in flow direction (Longest et al., 2013a). High flow nasal cannula (HFNC) oxygen delivery is a relatively new approach for ventilatory support in which heated and humidified air is delivered directly to the nasal cavity (Lee et al., 2013; Ward, 2013). Typical flow rates are in the range of approximately 10–60 LPM (Lee et al., 2013) in adults. Advantages of this technique include improved oxygenation compared with a face mask (Parke et al., 2011) and avoidance of the risks and costs associated with endotracheal tube intubation. However, aerosol delivery through nasal cannula devices is currently very inefficient even at low flow rates (Ari et al., 2011; Bhashyam et al., 2008) and clinically insufficient in many cases (Perry et al., 2013). As a result, aerosol delivery during HFNC ventilation gas support is selected in this study as a challenging case for device development and assessment of a high efficiency active DPI system employing controlled condensational growth technology.

The objective of this study is to develop an active DPI system for use with EEG particle formulations that can achieve high efficiency performance in terms of low depositional losses in the device and patient interface as well as high deaggregation of the powder. The initial case for evaluating the active DPI system is nose-to-lung aerosol delivery during HFNC ventilatory support. The system considered includes a flow control orifice and capsule chamber, 3D rod array, connective tubing, and previously optimized streamlined nasal cannula (Longest et al., 2013c). Variables of interest include the capsule piercing orientation, flow control orifice size, airflow rate, 3D rod array design, number of device actuations, and device coating. The previously optimized passive DPI developed by Behara et al. (2013b) is also considered operated in the active system. The potential of these new devices to achieve high efficiency aerosol delivery is evaluated as well as the production of aerosols that are small enough to likely pass through the nasal airways for effective nose-to-lung aerosol delivery.

2. Materials and Methods

2.1. Materials

Albuterol sulfate USP (AS) was purchased from Spectrum Chemical Co. (Gardena, CA) and Pearlitol® PF-Mannitol was donated from Roquette Pharma (Lestrem, France). Poloxamer

188 (Leutrol F68) was donated from BASF Corporation (Florham Park, NJ). L-leucine and all other reagents were purchased from Sigma Chemical Co. (St. Louis, MO). Hydroxypropyl methylcellulose (HPMC) capsules (size 3) were donated from Capsugel (Morristown, NJ).

2.2. Experimental setup

The experimental setup used in this investigation is shown in Fig. 1 and consisted of a manual ventilation bag to actuate the DPI, a flow meter (only required during experimental flow rate monitoring), the inline DPI, and an optional section of tubing connecting to a previously developed streamlined nasal cannula with separate inlets for aerosol delivery and high flow therapy (HFT) gas. Assembly of these units is referred to as the active DPI system. A standard 1.0 L ventilation bag (Adult Manual Resuscitator, Legend Medical Devices, South El Monte, California) was connected to the flow meter (Sensirion EM1, Sensirion AG, Stafa, Switzerland) which in turn was connected to the inline DPI devices under investigation. The aerosol particle size distribution exiting the nasal cannula was measured using a Next Generation Impactor (NGI; MSP Corp., Shoreview, MN) as detailed in Section 2.6. The flow meter was positioned between the bag and DPI devices and allowed monitoring of the real-time flow rate profiles generated during squeezing of the bag. A flow control orifice in the DPI was used to limit flow through the system and to create a jet of air in the capsule chamber that induced capsule vibration and initial fluidization of the powder. Flow control orifices with diameters of 3.6, 3.1, and 2.3 mm were selected to produce estimated maximum flow rates of 35, 30, and 15 LPM through the system. The ventilation bag was squeezed manually using two hands with a firm continuous pressure. Additional pressure on the bag was not found to significantly increase flow through the system due to the use of the flow control orifice. It is not expected that flow through the control orifice was sonic producing a choked flow limitation. Instead, a rapid rise in resistance at the measured flow for each orifice provided a practical maximum flow rate that could be achieved with manual activation.

The flow profile through the system was expected to have characteristic accelerating, plateau, and decelerating phases. Multiple metrics were used to characterize these transient profiles. First, total average flow rates were calculated as the time average of all recorded data points. A limitation of this approach is the expectation that a majority of aerosolization occurs during the plateau period, and not during the accelerating and decelerating phases. Therefore, this method likely underestimates the effective flow rate during a majority of aerosol formation. To address this issue, the root-mean-square (RMS) of the plateau flow rate was calculated, where the time points were evenly divided with a sampling time of 0.02 s. The beginning and end of the flow rate plateau were estimated to occur when 70% of the plateau average value was reached using an iterative process. The flow rate plateau was characterized by rapid oscillations arising from capsule vibrations. To characterize the upper range of velocity in the flow profile, the Q_{90} value was determined as the flow rate below which 90% of all measured values occurred. Finally, the maximum recorded velocity was also reported; which typically occurred only for an instant during a flow oscillation.

The ventilation bag was either squeezed until empty or until a total time of 5 s was reached. This time limit was implemented as the maximum time that a patient could inhale at a flow rate of approximately 45 LPM to receive the aerosol resulting in a total inhaled volume of 3.75 L.

2.3. DPI designs and capsule piercing

The four DPIs developed in this study are illustrated in Fig. 2 for connecting in-line with the mechanical ventilation system using standard 10 mm diameter tubing. An internal friction fit was used at the flow passage outlet to prevent flow disruption (Longest et al., 2013a) and minimize aerosol loss at this connection. A primary feature of the device is the 3D rod array design used to deaggregate the powder. This flow passage design was shown to maximize the NDSD parameter, which was proven to quantitatively correlate with deaggregation for a EEG formulation across a series of eight inhalers evaluated at multiple flow rates (Longest et al., 2013b). Briefly, the NDSD parameter captures the relative effects of turbulent energy, inverse of the turbulent eddy length scale, and exposure time to turbulence, which each play a role in the deaggregation of carrier-free powders (Longest et al., 2013b). The array implements 0.5 mm stainless steel rods in a staggered parallel arrangement where the flow accelerated between the rods in one row impinges on the rods in the next row. All designs had three rows of rods with a centerline distance between the rows of 1.75 mm and a rod length of 2.14 mm. Different combinations of flow control orifice sizes and rod patterns were used to create the four inhalers. The naming convention of the devices was based on the flow control orifice size and rod array structure. For example, the 3.6–565 device combined a 3.6 mm flow control orifice with a rod pattern that had 3 rows containing 5, 6, and 5 rods, respectively. Expected flows through each orifice were matched with rod array numbers (and therefore array cross-sectional dimensions) that would maintain an approximate similar velocity, and expected NDSD, through the array of each device. In all cases, the capsule chamber had a length and diameter of 19.6 and 7.5 mm, respectively.

The initial DPI design was the 3.6–565 device with a 13 cm length of tubing connecting the DPI to the nasal cannula inlet (Fig. 3a). Initial results indicated a relatively high amount (~10%) of depositional loss in the tubing of this configuration. As a result, the remaining designs minimized the connective tubing (~ 1 cm or no tubing) in joining the DPI to the nasal cannula (Fig. 3b).

The previous studies of Behara et al. (2013b) developed a 3D rod array DPI for oral inhalation that oriented the capsule chamber at an angle of 90° to the flow passage. It was shown that the 90° capsule chamber orientation accelerated the flow entering the 3D rod array and thereby further increased turbulence, NDSD, and resulting deaggregation. In the current study, the developed CC_{90}-3D inhaler was connected directly to the nasal cannula (Fig. 4) for comparison with the inline devices shown in Fig. 2. To operate the CC_{90}-3D inhaler in an active mode, the 10 mm diameter tubing from the ventilation bag was attached directly to the top of the capsule chamber. A short prototyped connector was then used to join the inhaler to the nasal cannula.

The inhalers were created using Autodesk Inventor and exported as .STL files to be prototyped. The files were then prepared using 3D Lightyear File Preparation Software. The

parts were built using a 3D Systems Viper SLA System (3D Systems Inc., Rock Hill, SC) using Accura 60 stereolithography resin (3D Systems Inc.). Once the parts were prototyped, they were cleaned using a Proclean SL Part Washer (3D Systems Inc.) and dried in 3D Systems dryer for 90 minutes.

The previous studies of Behara et al. (2013a, 2013b) have demonstrated that capsule piercing locations can affect both ED and aerosol size for EEG formulations. In this study, five capsule piercing cases were considered, as illustrated in Fig. 5. Each capsule was pierced twice (once in the head and once in the base) using a 0.5 mm needle and a custom-made capsule jig with pre-positioned hole locations (Behara et al., 2013b). The piercing apertures were located either at the top (or bottom), midway the head (or base) curvature, and at the start of the head (or base) curvature. In previous studies, a 0.5 mm aperture size provided both sufficient ED and final deaggregated aerosol size.

2.4. Nasal cannula design

As described, aerosol delivery during HFNC therapy is considered in this study with the active inline DPI systems. For aerosol administration in practice, the normal high flow nasal cannula used with gas delivery will be replaced with a divided cannula design as shown in Fig. 6 for simultaneous gas and aerosol delivery. The HFNC therapy gas (heated and humidified air stream) is then connected to the HFNC gas inlet of the divided cannula and enters the nose through one nasal prong. The aerosol is administered by connecting the active DPI system outlet to the aerosol inlet of the divided cannula. A streamlined flow passage is used to minimize loss in the cannula. An advantage of the divided cannula design is that the patient’s ventilatory support is maintained during aerosol administration as the aerosol and humidified gas flows can be delivered to separate nostrils, i.e., ECG nasal delivery. As described in previous studies by Longest et al. (2011) and Golshahi et al. (2013), this allows the aerosol to remain sufficiently small and bypass the nasal region. When the aerosol stream and HFNC gas combine in the nasopharynx, significant growth of the aerosol occurs resulting in an aerosol size that is expected to be retained in the lung airways. In the device naming convention, inline DPIs connected to the ECG nasal cannula are appended with the ECG suffix, e.g., 3.1–565-ECG.

2.5. Preparation of combination particle formulations

Enhanced excipient growth formulation combination particles were engineered as described by Son et al. (2013a). Briefly, a 20% ethanol in water mixture containing 0.5 %w/v of solutes consisting of AS, mannitol, L-leucine and poloxamer 188 in a ratio of 30:48:20:2 (%w/w) was spray dried using a Büchi Nano spray dryer B-90 (Büchi Laboratory-Techniques, Flawil, Switzerland). The powder formulation was generated using an airflow rate of 120 LPM, 100% liquid flow rate using the 4 μm nozzle diameter at an air inlet temperature of 70 °C. The air outlet temperature and spray dryer pressure were 40 °C and 35 mbar, respectively. Powder was collected from the electrostatic precipitator of the spray dryer and was stored in a desiccator until it was used. The powder yield was about 50–60%. Approximately 1 mg powder was dissolved in 100 ml of deionized water and was analyzed for content uniformity (n=3) of AS in the formulation using a validated HPLC method.

2.6. Particle size characterization

To determine particle size characteristics at the exit of the ECG cannula, 2 mg of formulation was filled in a HPMC size 3 capsule and was aerosolized into a NGI using the inline DPIs. The NGI flow rate was 60 LPM. The cannula was positioned centrally at the entrance of the pre-separator allowing the aerosol to be entrained into the impactor. All measurements were made with at least three replicates. The stages of the impactor were coated with silicone spray to minimize particle bounce and re-entrainment. The powders were aerosolized with the DPIs in a horizontal position; to assess the total aerosol size distribution, the USP induction port was not used. After aerosolization, the drug mass retained in the capsule, capsule chamber (CC), flow passage with 3D array, connective tubing, ECG cannula, and collected on the pre-separator, impaction plates and the filter was determined by washing each part with deionized water for quantitative HPLC analysis of albuterol sulfate.

2.7. Device retention and emitted dose

Emitted dose (ED) was calculated by subtracting the measured albuterol sulfate mass retained in the capsule, CC, flow passage, tubing and ECG cannula from the loaded dose, where the loaded dose was determined from the initial weight of the powder and percent of drug content in the EEG formulation. Fine particle fraction (FPF) of the EEG formulation ($FPF_{<5\mu m/ED}$) and sub-micrometer FPF ($FPF_{<1\mu m/ED}$) were defined as the percent mass of albuterol sulfate less than 5 μm and 1 μm, respectively, based on the mass percent ED. The albuterol sulfate mass median aerodynamic diameter (MMAD) was obtained for the drug mass entering the impactor. MMAD, $FPF_{<5\mu m/ED}$ and $FPF_{<1\mu m/ED}$ were calculated from linear regression equations resulting from cumulative percentage mass *vs.* natural logarithm of the cut-off diameter for the respective NGI stages.

2.8. Surface PTFE pre-treatment

In some cases, the capsule and device were coated with a commercial polytetrafluoroethylene (PTFE) suspension, which is a high contact angle (or low surface energy) material. A suspension of PTFE was sprayed inside the capsule, mouthpiece and CC to form a thin coating. Compressed air was blown through the coated portions until the surface appeared dry.

2.9. High-performance liquid chromatography (HPLC)

Albuterol sulfate was analyzed using a modular HPLC system (Waters Co., Milford, MA) with a Restek Allure PFP 15 × 3.2 mm column (Bellefonte, PA) connected to a 2996 PDA detector. An absorption wavelength of 276 nm was used in conjunction with Empower Pro software (Waters Corporation, Milford, MA) for data acquisition and analysis. The column was maintained at 25 °C. The analysis was conducted using isocratic analysis with 7:3 (v/v) methanol-20 mM ammonium formate in water (pH adjusted to 3.4 with 90% formic acid) at a flow rate of 0.75 ml min^{-1} and an injection volume of 100 μl.

2.10. Statistical analysis

In the current investigation, the data was expressed as the mean ± standard deviation (SD) based on three replicates of each experiment. The statistical significance was determined using one-way analysis of variance with Tukey's post-hoc analysis and between the groups using independent sample t-test at a P-value of 0.05 using SPSS (Version 21.0, SPSS, Inc., IL, USA).

3. Results

3.1. The effect of capsule piercing configuration on powder deaggregation

The capsule piercing configurations investigated in this study were presented in Fig. 5 as Cases 1–5. The capsule was loaded into the CC such that the air impinged directly on the body of the capsule. It was demonstrated by Behara et al. (2013b) that direct impingement of air onto a central aperture in the capsule reduced the deaggregation efficiency possibly due to less residence time of the powder in the capsule. In addition, it was demonstrated that the direction of air exiting the capsule had little effect on powder deaggregation (Behara et al., 2013b). In this study, Cases 1 and 2 were chosen for direct impingement of the air on the powder within the capsule, Case 3 was chosen for indirect flow into the capsule, Case 4 was previously used in Behara et al. (2013a) with a passive DPI where the capsule was oriented perpendicular to the incoming fluid (CC_1-3D), and Case 5 was the previous optimized alignment for CC_{90}-3D (Behara et al., 2013b); however, with Case 5 in this study, the orientation of the capsule aperture was reversed with the flow impinging directly on the capsule body.

The drug deposition and aerosolization performance of the AS EEG formulation following four actuations of the 1 L ventilation bag using the 3.1–565-ECG device is presented in Table 1 for Cases 1–5. The RMS average flow rate through the 3.1–565-ECG device was measured to be 27.2 LPM. Significantly lower ED was observed with Case 3 ($p=0.021$; Tukey's post-hoc) and Case 5 ($p=0.017$; Tukey's post-hoc) compared to Case 1; however, all ED values were >70%. Among the cases considered, Case 2 showed the highest ED and lowest capsule chamber retention. This is likely because of the direct impingement of the incoming flow on the capsule inlet aperture of Case 2, which minimizes powder residence time in the capsule and improves emptying. The capsule and CC retentions were highest with Case 5 compared to Case 1. Insignificant differences were observed among the piercing cases in flow passage, tubing and cannula drug retention. In general, significant differences were observed in relation to deaggregation [$FPF_{<5\mu m/ED}$ ($p=0.038$; one-way ANOVA) and $FPF_{<1\mu m/ED}$ ($p=0.013$; one-way ANOVA)]. The MMADs with Cases 1 and 2 were above 1.5 μm, while for Cases 3–5 the MMADs were less than 1.5 μm with $FPF_{<5\mu m/ED}$ over 80%. The aerosolization performance for Case 3 resulted in the highest $FPF_{<1\mu m/ED}$ (over 30%) and smallest MMAD of 1.39 μm. Case 3 therefore provided the best deaggregation of the powder with an acceptable ED of >70%. As a result of this high efficiency performance, the remainder of the experiments were carried out with Case 3 piercing in the DPIs.

3.2. Effect of flow control orifice size on deaggregation

In order to investigate the effect of flow control orifice size on aerosolization behavior of the AS EEG formulation, 3.6 and 3.1 mm orifice sizes were selected. Flow profile metrics for the 3.6–565-ECG and 3.1–565-ECG devices are reported in Table 2. The total average flow, RMS and Q_{90} values as well as maximum flow recorded and duration of actuation are provided. Duration of the total average and Q_{90} values represents total time to empty the bag, whereas duration of the RMS profile represents the timescale of the plateau period estimated as time where the flow is within 90% of the RMS average. As expected, decrease in orifice size resulted in a decrease in the flow rate and increased the bag squeeze duration. Use of the 3.1–565 inline DPI was observed to reduce the average flow rate (RMS of 3.5–565 = 35.2 LPM vs. RMS of 3.1–565 = 27.2 LPM). In all cases, the duration of actuation was less than 2 seconds, which is consistent with aerosol delivery over one inhalation per bag actuation.

It was questioned whether the increased flow rates produced with the 3.6–565 device compared with the 3.1–565 device would increase the deaggregation of the aerosol, and whether Case 3 piercing would result in optimal deaggregation for the 3.6–565 device. To address these issues, aerosolization characteristics were evaluated for the 3.6–565-ECG device with capsule piercing Cases 1–3, and the results were shown in Table 3. The EDs for the 3.6–565-ECG device (Table 3) were lower than those observed previously with the 3.1–565-ECG device (Table 1) partly due to the presence of the long connector tubing with the 3.6–565 device. However, the effect of the flow control orifice can also be observed upstream of the connecting tube, with high capsule retention observed for Cases 1 and 3, respectively. Variability in ED was also higher with the 3.6–565-ECG device vs. 3.1–565-ECG. Considering deaggregation behavior for the 3.6–565 device (Table 3), the trends were similar among Cases 1–3 as those observed for 3.1–565 in terms of $FPF_{<5\mu m/ED}$, $FPF_{<1\mu m/ED}$ and MMAD. However, the MMADs with the 3.1 mm device were 81.9, 73.9 and 81.3% lower for Case 1, Case 2, and Case 3, respectively, compared to the 3.6 mm device. The higher deaggregation efficiency with the 3.1 mm device could be a result of higher velocities through the smaller diameter orifice striking the capsule and affecting the initial powder fluidization process. Equally, the lower flow rate of the 3.1 mm device could result in a higher residence time of the aerosol in the 3D rod array, which is an effect previously shown to increase deaggregation (Longest et al., 2013b). These studies emphasize the fact that capsule piercing and air inlet aperture size are critical in the development of DPIs. Based on optimal performance in the experiments conducted to this point, further investigations are conducted with the 3.1–565-ECG device and Case 3 piercing.

3.3. Effect of number of ventilation bag actuations

The effect of the number of ventilation bag actuations on the emitted dose and deaggregation efficiency for the 3.1–565-ECG device is presented in Table 4. Results for two actuations in Table 4 are compared with results for four actuations from Table 1 (indicated in grey text). There were insignificant differences in ED and deaggregation of AS between two and four actuations of the ventilation bag. However, the variability associated with two squeezes was 2.5, 6.3, 3.9 and 2.1 fold higher for ED, $FPF_{<5\mu m/ED}$, $FPF_{<1\mu m/ED}$

and MMAD, respectively, compared to four squeezes. Despite this increase in variability, the relative standard deviation remained low for both ED (3.5%) and MMAD (7.4%) using two actuations. The variability increase with two actuations could mainly be attributed to the volume of air passing through the system that detaches the adhered particles from the device component surfaces. In order to evaluate this theory, further investigations were focused on coating the device and capsule with low surface energy PTFE to examine the effects on emptying and deaggregation of AS with two actuations.

3.4. Effect of capsule and device coating with PTFE

The effect of PTFE coating on ED and deaggregation for the 3.1–565-ECG device is presented in Table 5 for two bag actuations. Significantly higher ED ($p=0.018$; independent sample t-test) was obtained from the device coated with PTFE (ED = 78.2%) compared to uncoated (ED = 72.1%). There was no significant difference in de-aggregation ($FPF_{<5\mu m/ED}$, $FPF_{<1\mu m/ED}$ and MMAD) between coated and uncoated devices. However, coating was observed to largely reduce variability in both ED and deaggregation parameters. For example, the relative standard deviation for the ED with PTFE coating was 1.1%. Similar results are observed for the variability in MMAD with PTFE coating of the device and capsule.

3.5. Comparison between inline and CC_{90}-3D devices

The efficiency of the 3.1–565-ECG device was compared with the previously developed CC_{90}-3D inhaler with results presented in Table 6. As shown in Fig. 4, the flow passage and streamlined ECG cannula served as a single unit for the CC_{90}-3D inhaler. Both devices employed the previously optimized capsule piercing configurations. In order to better compare these two devices, a 3.1 mm flow control orifice was used with the CC_{90}-3D inhaler (whereas the original study of Behara et al. (2013b) implemented an optimal orifice size of 4.06 mm to allow for inhalation at 45 LPM with a pressure drop of 4 kPa). In order to facilitate comparison of the data, the aerosolization efficiency of 3.1–565-ECG was taken from Table 1 (indicated with grey text) and presented against the CC_{90}-3D data in Table 6 for the case of 4 actuations. The ED was significantly higher ($p=0.026$; independent sample t-test) with 3.1–565-ECG (71.1%) compared to CC_{90}-3D (66.4%) when actuated in the present active mode. In comparing the deaggregation, insignificant differences were observed between the devices in $FPF_{<1\mu m/ED}$ and MMAD. Both the devices showed $FPF_{<5\mu m/ED}$ over 80%; however, CC_{90}-3D showed a small but statistically significantly higher $FPF_{<5\mu m/ED}$ ($p=0.045$; independent sample t-test). Although the orifice size and 3D array pattern between the devices were the same, the dimensions of the CC and flow passage were different. The CC and flow passage dimensions are more narrow with 3.1–565-ECG in comparison with the CC_{90}-3D inhaler. In addition, the CC design of CC_{90}-3D was semicircular while that of 3.1–565-ECG was circular. These differences could have contributed to lower ED with the CC_{90}-3D inhaler and highlight that these devices perform best when used as intended. However, the CC_{90}-3D inhaler still performed well and could be equivalent to the inline device if the ED were increased, perhaps by using surface coating as described previously.

3.6. Effect of 3D array pattern on AS deaggregation

In comparing the 3.6 mm and 3.1 mm orifice devices, the smaller orifice achieved lower flow rates (Table 2) and produced longer durations of bag emptying. However, the effect of 3D array number pattern on emptying and deaggregation is not known. In order to investigate the effect of the 3D rod array, 2.3–343-ECG and 2.3–212-ECG devices were designed and tested. The flow profiles for 2.3–343-ECG and 2.3–212-ECG are reported in Table 7. It was recognized that decreasing the orifice size from 3.1 mm (Table 2) to 2.3 mm (Table 7) decreased the flow rate metrics (e.g, 3.1–565 mm RMS = 27.2 LPM vs. 2.3–343 RMS = 14.7 LPM). In addition, implementing the smaller rod array (212) increased the total device resistance thereby reducing the flow rate with an RMS flowrate value for 2.3–212 of 11.6 LPM. In all cases, the maximum duration of bag emptying was 3.5 s, which is within a reasonable inhalation period for receiving the aerosol during slow and deep inspiration.

Emitted dose and aerosolization characteristics for the 2.3–343-ECG and 2.3–212-ECG devices are reported in Table 8 and compared with results for 3.1–565-ECG (in grey) from Table 1. Four bag actuations were used in all cases with optimal (Case 3) capsule piercing. Compared to 3.1–565-ECG, both 2.3 devices have insignificant differences in ED; however, the deaggregation efficiency of 3.1–565-ECG was higher compared with the 2.3 devices likely due to higher RMS velocity and increased turbulence (Table 2 vs. Table 7). The mean RMS flow rates for the 3.6–565-ECG, 2.3–343-ECG and 2.3–212-ECG devices were 27.2, 14.7 and 11.6 LPM, respectively. In contrast, the mean squeeze duration was 36% (2.3–212-ECG) and 82% (2.3–343-ECG) longer than with 3.1–565-ECG. In comparing the 2.3 mm orifices with 343 and 212 rod arrays, insignificant differences (independent sample t-test) were observed in ED and deaggregation. However, the variability associated with 2.3–212-ECG was higher than with 2.3–343-ECG.

4. Discussion

A high efficiency DPI should provide a high ED, operate efficiently at low flow rates, provide low depositional device losses, and effectively deaggregate the powder to disperse the aerosol into its primary particles. However, these characteristics are typically difficult to achieve at the same time in a device. For example, increasing the flow rate typically improves deaggregation of the powder, but also results in increased depositional losses in the device, patient interface, and patient extrathoracic airways. Ideally, a DPI should provide effective deaggregation at relatively low flow rates inhaled by the patient, which minimizes depositional losses and maximizes lung delivery. In the current study, capsule piercing configurations were shown to influence ED and deaggregation with Case 3 providing the best deaggregation efficiency. However, Cases 1 and 2 achieved higher EDs (near 80%) with only a small increase in the aerosol MMAD for the 3.1–565 device. By controlling the size of the flow control orifice, overall performance of the inline DPI was improved. For example, reducing the flow control orifice diameter from 3.6 mm (Table 3) to 3.1 mm (Table 1) with Case 3 piercing, the ED and deaggregation were significantly increased. Reducing the orifice size further from 3.1 to 2.3 mm decreased the flow rate (RMS reduced from 27.2 to 14.7 LPM) and had no significant effect on the emitted dose, but deaggregation efficiency was reduced. Variability in the ED and deaggregation metrics was low for devices

with an orifice size of 3.1 mm and below; however, implementing four actuations instead of two provided the lowest relative standard deviations. Overall, the devices that provided the best combination of performance were the 3.1–565 and 2.3–343 inline DPIs. For high flow rate applications (~30 LPM), the 3.1 device achieved an ED = 71.1% with a $FPF_{<5\mu m/ED}$ = 83.1%, and MMAD = 1.39 μm. Applying PTFE coating to this device increased the ED to near 80% and achieved high efficiency performance as defined by Behara et al. (2013b) for passive hand-held devices. For lower flow applications (~15 LPM), the 2.3 mm device performed nearly as well but demonstrated a small increase in MMAD. The basis for defining high efficiency metrics is expected low depositional losses in the patient interface and extrathoracic airways with high delivery efficiency to the lungs. At the lower flow rate provided by the 2.3–343 device, these depositional losses may be equal to or lower than the 3.1–565 device. Therefore, comparing these two devices further will require consideration of specific applications and the inclusion of extrathoracic airway models, as performed by Golshahi et al. (2013) for nebulized submicrometer aerosols and nose-to-lung aerosol delivery.

As described in the Introduction, very few studies have evaluated the delivery of dry powder aerosols during mechanical ventilation. However, there are a number of advantages to this approach including stable formulations, inexpensive devices, and the potential to deliver large doses of medication to the lungs. The nose to lung aerosol administration case study of Laube et al. (2012) achieved an ED of approximately 90% from the insufflator; however, a majority of the dose was lost in the device with 0.3–4% reaching the lungs of an *in vitro* infant model. In the current study, one of the best performing devices (3.1–565-ECG with PTFE coating) achieved an ED of 78.2% from the cannula with a $FPF_{<5\mu m/ED}$ = 78.9% and an MMAD of 1.47 μm. Higher flow rates were employed in the current study compared with the study of Laube et al. (2012). However, results indicate that reducing the flow rate may improve performance of deaggregation with the active DPI systems due to use of the 3D rod array. Considering the emitted dose, the developed inhalers improved ED from the delivery system by a factor of approximately 3–12 fold compared with the Laube et al. (2012) study. The previous study of Golshahi et al. (2013) demonstrated that initially small particles used with EEG delivery were able to effectively penetrate the nasal airways. As a result, the improved delivery efficiency from the current designs is expected to translate to large improvements in lung dose. However, future studies are needed to investigate the nasal depositional losses of the current nose-to-lung delivery strategy and to determine if these improvements can be translated to infant and pediatric subjects as well.

Active DPIs often employ complex methods to aerosolize the powder. For example, the Spiros® device implements battery operated rotating blades to fluidize and deaggregate the aerosol. As reviewed by Harper et al. (2007), the Exubera® device uses a compressed air source and a well designed flow channel. Similarly, the continuous powder aerosolizer of Pohlmann et al. (2013) implements repeated pulses of air for producing the aerosol. Ultrasound and other vibration inducing techniques are also available for active deaggregation (Corcoran et al., 2013; Crowder and Hickey, 2006). In comparison, the deaggregation mechanism of the current 3D rod array implements no moving parts. By maximizing high turbulent energy in the small eddies, represented as high NDSD, high

efficiency deaggregation is achieved. In part, the high efficiency performance of the active DPI systems considered in this study is due to the highly dispersible EEG formulation. However, Son et al. (2013b) previously considered the same EEG formulation in the active Spiros and Exubera devices. Aerosolization characteristics for Spiros were ED = 73.7% and MMAD = 2.6 μm. For Exubera, aerosolization characteristics were ED = 62.8% and MMAD = 2.0 μm. Compared with these products, the proposed simple active DPI systems developed in this study demonstrate reduced MMAD and equal or improved ED at a likely reduced cost.

In comparison with other recently developed 3D rod array DPIs, the aerosolization performance of the inline active DPI is only marginally reduced. Studies by Behara et al. (2013a, 2013b) report two new 3D rod array devices for oral inhalation that met the previously defined high efficiency performance criteria at an operating flow rate of approximately 45 LPM. In comparison, the selected best performing 3.1–565 (with PTFE) and 2.3–343 devices of this study had slightly lower $FPF_{<5\mu m/ED}$ (65.4–78.9) and higher MMADs (1.47–1.64 μm). This may be due in part to the lower flow rate used with the inline devices. Specifically, the RMS for the best two performing inline devices was in the range of 14.7–27.2 LPM. These lower flow rates with the inline active devices are required for practical delivery to one nostril during nose-to-lung delivery with HFNC therapy. In the current study, the CC_{90}-3D inhaler of Behara et al. (2013b) was also tested in active mode with a 3.1 mm orifice and effective flow rate of approximately 30 LPM. As shown in Table 6, at an equal flow rate, the inline device was more efficient than the previously developed inhaler when both were used in the active DPI system. This small reduction in performance of the CC_{90}-3D inhaler was not observed at a lower flow rate as considered by Behara et al. (2013b), so it is likely due to positive pressure in the capsule chamber and an altered pressure profile through the device during active operation compared with the previous consideration of passive inhalation. As a result of these observations, it appears that the inline devices are the most effective when operated in a mechanical ventilation system in an active mode (i.e., with positive pressure).

The use of active DPIs in mechanical ventilation systems was previously discussed by Dhand (2005). While the advantage of DPI delivery was apparent during mechanical ventilation, Dhand (2005) pointed out that the major limitation of the system was the use of humid air in the ventilator, which is known to decrease DPI performance. In the current study, two delivery lines were used for the administration of aerosols during HFNC therapy such that passing the high humidity heated airflow from the high flow therapy generator through the inline DPI was avoided. With ECG nose-to-lung delivery, the aerosol and humidity streams remain separate until the aerosol has passed a majority of the nasal cavity with low deposition. It is expected that the delivery of room air at a flow rate <30 LPM through the aerosol delivery line over 2–4 bag actuations corresponding to 2–4 deep nasal inspirations will be well tolerated by the patient. The delivery of the heated and humidified air remains in place such that the patient continues to receive ventilatory support. In addition, the humidified air provides the source of water vapor required for droplet size increase and lung deposition with ECG delivery. Similar DPI systems could be adapted for use during other forms of noninvasive and invasive mechanical ventilation.

Limitations of the current study include the absence of a nasal geometry, consideration of one loaded DPI dose weight, and evaluation of one drug formulation. The objective of this initial study was to evaluate the performance of the newly proposed active DPI systems in terms of ED and aerosolization performance. A nasal model is now required to determine if the aerosols produced and flow rates are sufficiently small to allow for effective nose-to-lung delivery for the active DPI systems. Only one loaded DPI dose weight (2 mg) was considered in the current study. Higher dose weights may require additional bag actuations for high EDs. However, this is expected to be well tolerated considering that the ventilation support remains in place and the active device employs room-condition air, which is not expected to overly dry the nasal airways. Finally, AS was considered as a model drug that has been optimized in terms of a spray dried EEG formulation of submicrometer primary particles (Son et al., 2013a). Consideration of other therapeutic molecules will require additional spray drying optimization work; however, limited experience with other molecules (terbutaline sulfate and ciprofloxacin hydrochloride) indicate that this is feasible.

Conclusions

In conclusion, high efficiency active DPI systems were developed and their use demonstrated with flow rates as low as approximately 10 LPM. The two best performing designs achieved ED > 70% with $FPF_{<5\mu m/ED}$ as high as 80% and MMADs of approximately 1.5 μm. A flow control orifice was used to limit flow through the device and provide highly reproducible flow rates from the manually actuated bag. Controlling the orifice size alters the dispersion flow rate and can be used to improve deaggregation performance. Coating the device and capsule with PTFE was found to increase the ED to approximately 80%. These devices can be implemented in a number of applications where active DPIs are needed including mechanical ventilation systems such as HFNC therapy, for nose-to-lung aerosol delivery, for patients that may not be able to generate reproducible or sufficient flow rates for effective aerosol delivery, and in test animals. Future studies are needed to evaluate nasal deposition for the HFNC and nose-to-lung applications, higher doses, different medications, and other delivery scenarios.

Acknowledgments

The authors gratefully acknowledge the financial support from the National Heart, Lung, and Blood Institute by Award R01 HL107333. The content is solely the responsibility of the authors and does not necessarily represent the official views of the National Heart, Lung, and Blood Institute or the National Institutes of Health.

References

Ari A, Fink JB. Inhalation therapy in patients receiving mechanical ventilation: an update. Journal of Aerosol Medicine and Pulmonary Drug Delivery. 2012; 25:319–332. [PubMed: 22856594]

Ari A, Harwood R, Sheard M, Dailey P, Fink JB. In vitro comparison of heliox and oxygen in aerosol delivery using pediatric high flow nasal cannula. Pediatric Pulmonology. 2011; 46:795–801. [PubMed: 21438178]

Behara SRB, Farkas D, Hindle M, Longest PW. Development of a high efficiency dry powder inhaler: Effects of a new capsule orientation and surface coatings. Pharmaceutical Research. 2013a; 30:1608–1627. [PubMed: 23471640]

Behara SRB, Farkas DR, Hindle M, Longest PW. Development and comparison of new high efficiency dry powder inhalers for carrier-free formulations. Journal of Pharmaceutical Sciences. 2013b (in press).

Bhashyam AR, Wolf MT, Marcinkowski AL, Saville A, Thomas K, Carcillo JA, Corcoran TE. Aerosol delivery through nasal cannulas: An in vitro study. Journal of Aerosol Medicine and Pulmonary Drug Delivery. 2008; 21:181–187. [PubMed: 18518794]

Concessio NM, JagerWaldau R, Hickey AJ. Aerosol delivery from an active emission multi-single dose dry powder inhaler. Particulate Science And Technology. 1997; 15:51–63.

Corcoran TE, Venkataramanan R, Hoffman RM, George MP, Petrov A, Richards T, Zhang S, Choi J, Gao YY, Oakum CD, Cook RO, Donahoe M. Systemic Delivery of Atropine Sulfate by the MicroDose Dry-Powder Inhaler. Journal Of Aerosol Medicine And Pulmonary Drug Delivery. 2013; 26:46–55. [PubMed: 22691110]

Crowder T, Hickey A. Powder specific active dispersion for generation of pharmaceutical aerosols. International Journal Of Pharmaceutics. 2006; 327:65–72. [PubMed: 16930884]

Dhand R. Inhalation therapy with metered-dose inhalers and dry powder inhalers in mechanically ventilated patients. Respiratory Care. 2005; 50:1331–1344. [PubMed: 16185369]

Dhand R. Aerosol therapy in patients receiving noninvasive positive pressure ventilation. Journal of Aerosol Medicine and Pulmonary Drug Delivery. 2012; 25:63–78. [PubMed: 22191396]

Dolovich MB, Dhand R. Aerosol drug delivery: developments in device design and clinical use. Lancet. 2011; 377:1032–1045. [PubMed: 21036392]

Everard ML, Devadason SG, LeSouef PN. In vitro assessment of drug delivery through an endotracheal tube using a dry powder inhaler delivery system. Thorax. 1996; 51:75–77. [PubMed: 8658374]

Geller DE, Weers J, Heuerding S. Development of an inhaled dry-powder formulation of Tobramycin using PulmoSphereTM technology. Journal of Aerosol Medicine and Pulmonary Drug Delivery. 2011; 24:175–182. [PubMed: 21395432]

Golshahi L, Tian G, Azimi M, Son YJ, Walenga RL, Longest PW, Hindle M. The use of condensational growth methods for efficient drug delivery to the lungs during noninvasive ventilation high flow therapy. Pharmaceutical Research. 2013; 30:2917–2930. [PubMed: 23801087]

Grainger CI, Alcock R, Gard TG, Quirk AV, van Amerongen G, de Swart RL, Hardy JG. Administration of an insulin powder to the lungs of cynomolgus monkeys using a Penn Century insufflator. International Journal Of Pharmaceutics. 2004; 269:523–527. [PubMed: 14706262]

Harper NJ, Gray S, De Groot J, Parker JM, Sadrzadeh N, Schuler C, Schumacher JD, Seshadri S, Smith AE, Steeno GS, Stevenson CL, Taniere R, Wang M, Bennett DB. The design and performance of the Exubera((R)) pulmonary insulin delivery system. Diabetes Technology & Therapeutics. 2007; 9:S16–S27. [PubMed: 17563300]

Hindle M, Longest PW. Evaluation of enhanced condensational growth (ECG) for controlled respiratory drug delivery in a mouth-throat and upper tracheobronchial model. Pharmaceutical Research. 2010; 27:1800–1811. [PubMed: 20454837]

Hindle M, Longest PW. Condensational growth of combination drug-excipient submicrometer particles for targeted high efficiency pulmonary delivery: Evaluation of formulation and delivery device. J Pharm Pharmacol. 2012; 64:1254–1263. [PubMed: 22881438]

Islam N, Cleary MJ. Developing an efficient and reliable dry powder inhaler for pulmonary drug delivery - A review for multidisciplinary researchers. Medical Engineering and Physics. 2012; 34:409–427. [PubMed: 22277307]

Laube BL, Sharpless G, Shermer C, Sullivan V, Powell K. Deposition of dry powder generated by solovent in Sophia Anatomical infant nose-throat (SAINT) model. Aerosol Science and Technology. 2012; 46:514–520.

Lee JH, Rehder KJ, Williford L, Cheifetz IM, Turner DA. Use of high flow nasal cannula in critically ill infants, children, and adults: a critical review of the literature. Intensive Care Med. 2013; 39:247–257. [PubMed: 23143331]

LiCalsi C, Christensen T, Bennett JV, Phillips E, Witham C. Dry powder inhalation as a potential delivery method for vaccines. Vaccine. 1999; 17:1796–1803. [PubMed: 10194842]

Longest PW, Golshahi L, Hindle M. Improving pharmaceutical aerosol delivery during noninvasive ventilation: Effects of streamlined components. Annals of Biomedical Engineering. 2013a; 41:1217–1232. [PubMed: 23423706]

Longest PW, Hindle M. Numerical model to characterize the size increase of combination drug and hygroscopic excipient nanoparticle aerosols. Aerosol Science and Technology. 2011; 45:884–899. [PubMed: 21804683]

Longest PW, Hindle M. Condensational growth of combination drug-excipient submicrometer particles: Comparison of CFD predictions with experimental results. Pharmaceutical Research. 2012; 29:707–721. [PubMed: 21948458]

Longest, PW.; Hindle, M.; Xi, J. Effective delivery of nanoparticles and micrometer-sized pharmaceutical aerosols to the lung through enhanced condensational growth. International Patent Application. PCT/US2009/034360. 2009.

Longest PW, Son YJ, Holbrook LT, Hindle M. Aerodynamic factors responsible for the deaggregation of carrier-free drug powders to form micrometer and submicrometer aerosols. Pharmaceutical Research. 2013b; 30:1608–1627. [PubMed: 23471640]

Longest PW, Tian G, Hindle M. Improving the lung delivery of nasally administered aerosols during noninvasive ventilation - An application of enhanced condensational growth (ECG). Journal of Aerosol Medicine and Pulmonary Drug Delivery. 2011; 24:103–118. doi:110.1089/jamp.2010.0849. [PubMed: 21410327]

Longest PW, Walenga RL, Son YJ, Hindle M. High efficiency generation and delivery of aerosols through nasal cannula during noninvasive ventilation. Journal of Aerosol Medicine and Pulmonary Drug Delivery. 2013c; 26:266–279. [PubMed: 23273243]

Newman SP, Busse WW. Evolution of dry powder inhaler design, formulation, and performance. Respiratory Medicine. 2002; 96:293–304. [PubMed: 12113378]

Parke RL, McGuinness SP, Eccleston ML. A Preliminary Randomized Controlled Trial to Assess Effectiveness of Nasal High-Flow Oxygen in Intensive Care Patients. Respiratory Care. 2011; 56:265–270. [PubMed: 21255498]

Perry SA, Kesser KC, Geller DE, Selhorst DM, Rendle JK, Hertzog JH. Influences of Cannula Size and Flow Rate on Aerosol Drug Delivery Through the Vapotherm Humidified High-Flow Nasal Cannula System. Pediatr Crit Care Med. 2013; 14:E250–E256. [PubMed: 23628834]

Pohlmann G, Iwatschenko P, Koch W, Windt H, Rast M, Gama de Abreu M, Taut FJH, De Muynck C. A novel continuous powder aerosolizer (CPA) for inhalative administration of highly concentrated recombinant surfactant protein-C (rSP-C) surfactant to perterm neonates. Journal of Aerosol Medicine and Pulmonary Drug Delivery. 201310.1089/jamp.2012.0996

Smith IJ, Bell J, Bowman N, Everard M, Stein S, Weers JG. Inhaler Devices: What Remains to be Done? Journal Of Aerosol Medicine And Pulmonary Drug Delivery. 2010; 23:S25–S37. [PubMed: 21133798]

Son YJ, Longest PW, Hindle M. Aerosolization characteristics of dry powder inhaler formulations for the excipient enhanced growth (EEG) application: Effect of spray drying process conditions on aerosol performance. International Journal of Pharmaceutics. 2013a; 443:137–145. [PubMed: 23313343]

Son Y-J, Longest PW, Tian G, Hindle M. Evaluation and modification of commercial dry powder inhalers for the aerosolization of submicrometer excipient enhanced growth (EEG) formulation. Eur J Pharm Sci. 2013b; 49:390–399. [PubMed: 23608613]

Tang P, Chan HK, Rajbhandari D, Phipps P. Method to Introduce Mannitol Powder to Intubated Patients to Improve Sputum Clearance. Journal Of Aerosol Medicine And Pulmonary Drug Delivery. 2011; 24:1–9. [PubMed: 20961167]

Tian G, Longest PW, Li X, Hindle M. Targeting aerosol deposition to and within the lung airways using excipient enhanced growth. Journal of Aerosol Medicine and Pulmonary Drug Delivery. 2013; 26:248–265. [PubMed: 23286828]

Tian G, Longest PW, Su G, Hindle M. Characterization of respiratory drug delivery with enhanced condensational growth (ECG) using an individual path model of the entire tracheobronchial airways. Annals of Biomedical Engineering. 2011; 39:1136–1153. [PubMed: 21152983]

Ungaro F, De Rosa G, Miro A, Quaglia F, La Rotonda MI. Cyclodextrins in the production of large porous particles: Development of dry powders for the sustained release of insulin to the lungs. Eur J Pharm Sci. 2006; 28:423–432. [PubMed: 16806857]

Ward JJ. High-Flow Oxygen Administration by Nasal Cannula for Adult and Perinatal Patients. Respiratory Care. 2013; 58:98–120. [PubMed: 23271822]

Weers JG, Bell J, Chan HK, Cipolla D, Dunbar C, Hickey AJ, Smith IJ. Pulmonary Formulations: What Remains to be Done? Journal Of Aerosol Medicine And Pulmonary Drug Delivery. 2010; 23:S5–S23. [PubMed: 21133800]

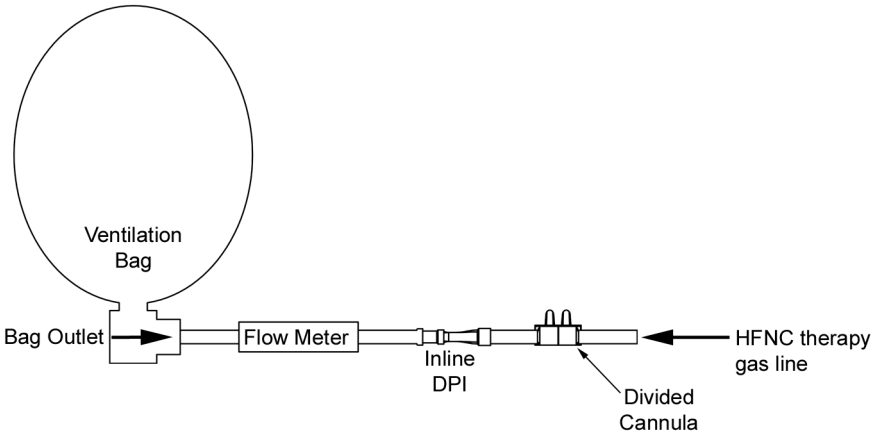

Figure 1.

The active dry powder inhaler (DPI) system including a ventilation bag, flow meter (for experimental testing only), inline DPI (containing a flow control orifice and 3D rod array), and streamlined nasal cannula.

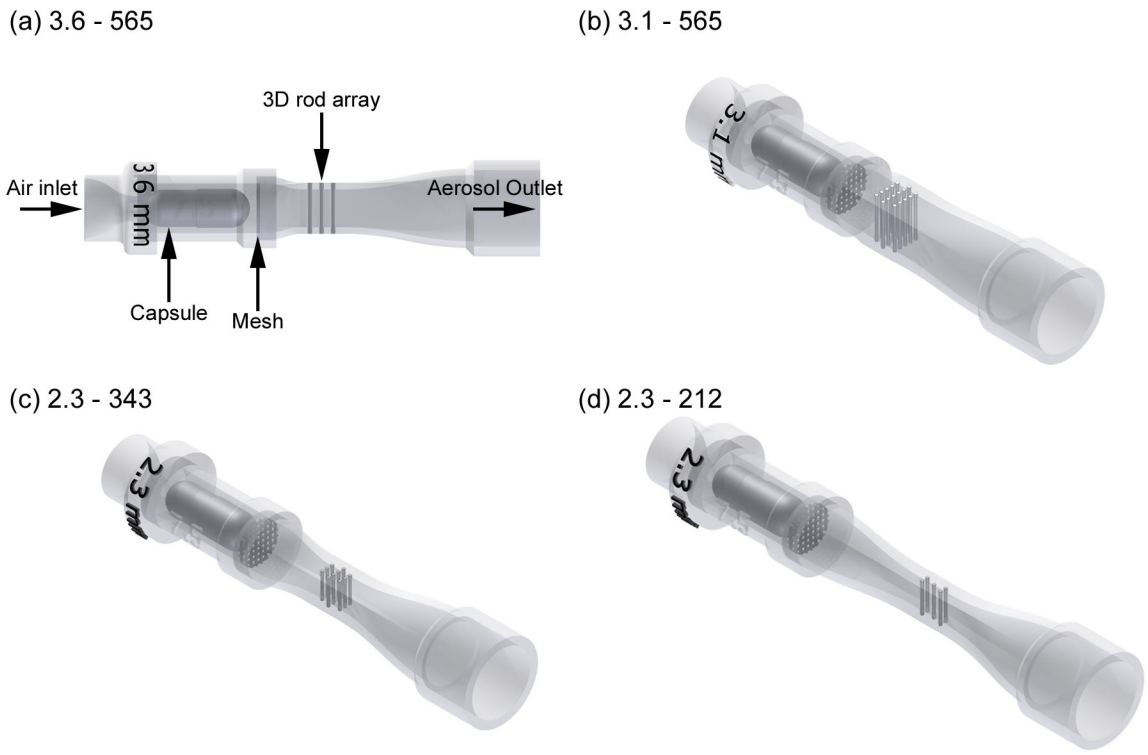

Figure 2.

Inline DPI devices consisting of a flow control orifice (3.6 - 2.3 mm diameter), capsule chamber, restraining mesh, 3D rod array and flow passage that connects to 10 mm diameter ventilator tubing. Different flow control orifice size and rod array pattern configurations were considered including (a) 3.6 mm orifice and 5-6-5 rod array pattern, (b) 3.1 mm orifice and 5-6-5 rod array pattern, (c) 2.3 mm orifice and 3-4-3 rod array pattern, and (d) 2.3 mm orifice and 2-1-2 rod array pattern.

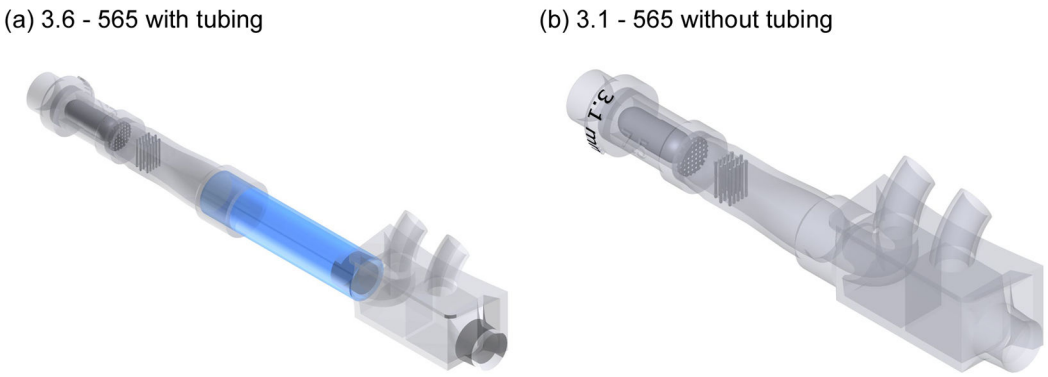

Figure 3.

Illustration of the DPI (a) with and (b) without connective tubing leading to the ECG cannula. The length of the connective tubing in Panel (a) is not draw to scale. In the experiments, only the 3.6–565 DPI contained a 13 cm length of 10 mm diameter connective tubing between the device and ECG cannula. The other devices implemented a much shorter (~1 cm) length or eliminated the connective tubing.

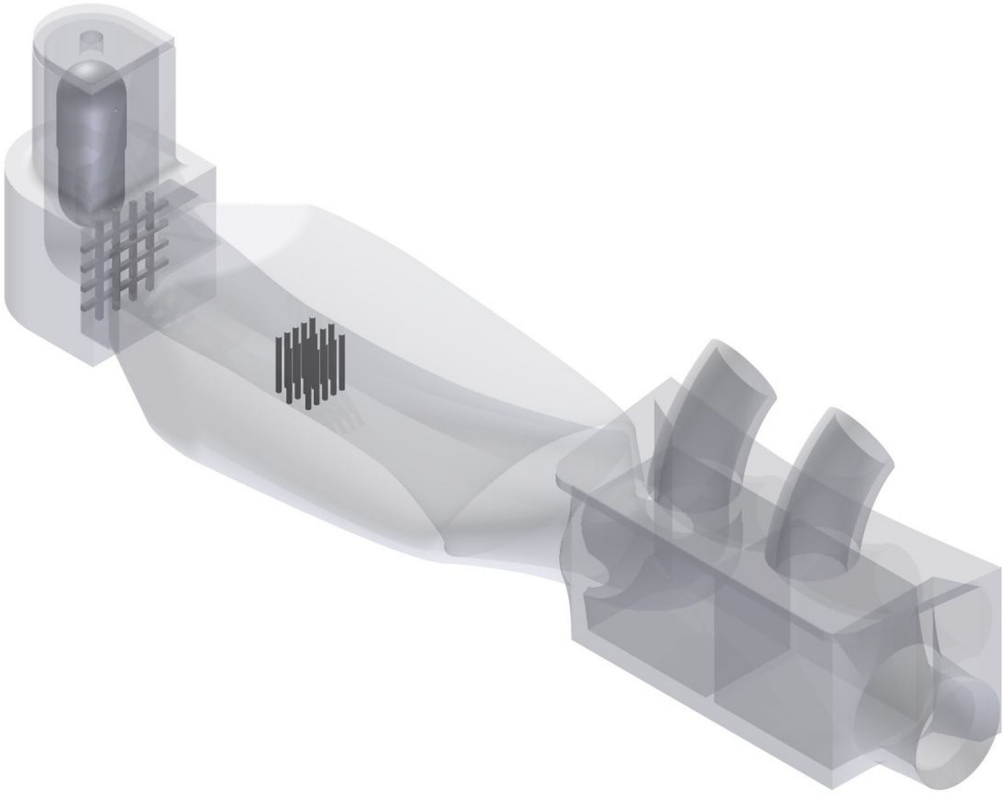

Figure 4.

Connection of the previously optimized passive CC_{90}-3D inhaler used for oral inhalation to the ECG cannula. In this setup, the CC_{90}-3D inhaler was operated by connecting the flow delivery line to the inlet orifice above the capsule chamber.

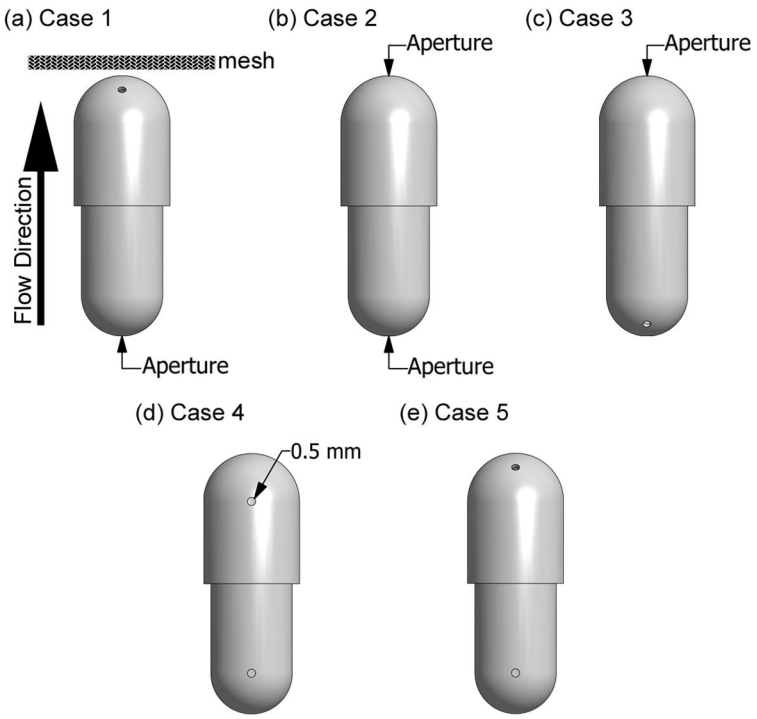

Figure 5.

Capsule piercing apertures with different configurations denoted (a) Case 1, (b) Case 2, (c) Case 3, (d) Case 4, and (e) Case 5. Direction of flow during operation and the restraining mesh are illustrated in Panel (a). Apertures with a diameter of 0.5 mm were located at the top (or bottom) of the capsule, midway the head (or base) curvature, and at the start of the head (or base) curvature.

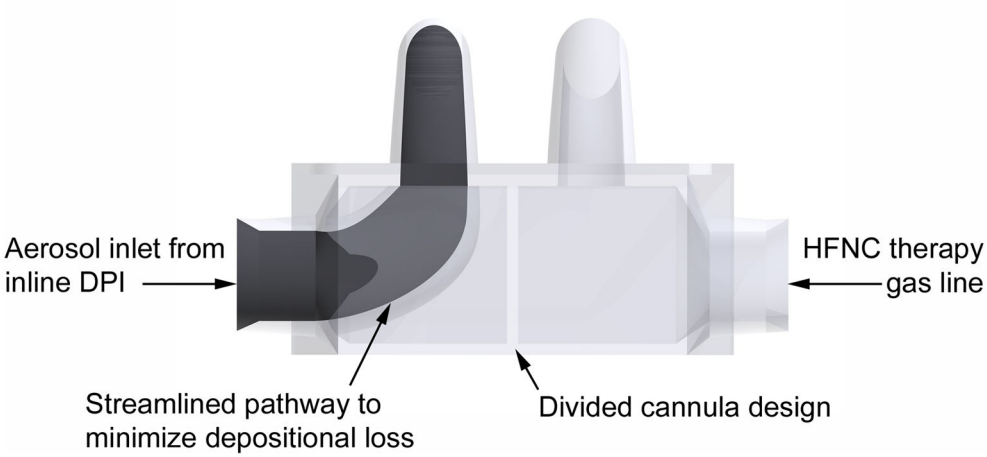

Figure 6.

Divided ECG cannula for dual stream aerosol delivery during HFNC therapy. During aerosol administration, the aerosol stream from the DPI enters one side of the cannula and flows through a streamlined passage into one nasal prong. High flow therapy (heated and humidified) gas enters the other nasal prong.

Table 1

The effect of capsule piercing configuration on the mean AS device retention and aerosolization performance at the exit of the ECG cannula for five different cases as presented in Fig. 5 when the 1 liter bag was squeezed four times through 3.1–565-ECG device. The device was connected to a streamlined ECG cannula positioned at the entrance to the NGI. The standard deviation (SD) is shown in parenthesis [n=3].

Description	Case 1	Case 2	Case 3	Case 4	Case 5
ED (%)*	76.5 (0.9)	79.2 (0.7)	71.1 (1.0)**	73.9 (2.4)	70.9 (2.6)**
Capsule (%)*	7.1 (0.5)	6.3 (0.7)	8.5 (0.7)	7.5 (0.4)	9.5 (1.6)**
CC (%)*	3.3 (0.8)	1.2 (0.1)**	6.8 (1.0)**	4.7 (0.7)	7.6 (0.6)**
Flow passage (%)	8.7 (0.4)	8.8 (0.2)	9.6 (0.6)	9.1 (0.4)	8.2 (0.7)
Connecting tubing (~1 cm) (%)	1.8 (0.2)	1.8 (0.1)	1.6 (0.3)	1.5 (0.1)	1.6 (0.3)
ECG Cannula (%)	2.6 (0.3)	2.7 (0.2)	2.3 (0.2)	3.3 (2.0)	2.1 (0.0)
$FPF_{<5\mu m/ED}$ (%)*	78.1 (3.7)	71.6 (4.6)	83.1 (1.4)	81.8 (4.7)	80.4 (4.7)
$FPF_{<1\mu m/ED}$ (%)*	23.7 (2.7)	20.5 (2.3)	30.3 (1.6)	27.6 (3.3)	27.7 (3.9)
MMAD (μm)*	1.55 (0.06)	1.62 (0.04)	1.39 (0.05)**	1.48 (0.06)	1.45 (0.08)

*$P<0.05$ significant effect of capsule piercing on % ED, capsule and CC drug retention, $FPF_{<5\mu m/ED}$, $FPF_{<1\mu m/ED}$ and MMAD (one-way ANOVA).

**P<0.05 significant effect compared to Case 1 (post-hoc Tukey).

Table 2

Flow profiles for the 3.6–565-ECG and 3.1–565-ECG devices based on total average flow, RMS, and Q_{90} metrics [n≥3; mean (SD)]. The maximum instantaneous flow rate recorded is also reported.

Method	3.6–565-ECG			3.1–565-ECG		
	Flow rate (LPM)	**Duration (s)**	**Maximum flow (LPM)**	**Flow rate (LPM)**	**Duration (s)**	**Maximum flow (LPM)**
Total average	25.4 (1.6)	1.1 (0.2)	40.9 (2.6)	21.5 (1.8)	1.7 (0.3)	37.7 (2.4)
RMS	35.2 (1.9)	0.7 (0.1)		27.2 (1.9)	1.1 (0.0)	
Q_{90}	39.6 (2.2)	1.1 (0.2)		33.0 (2.3)	1.7 (0.3)	

Total average: Average of all flow values for entire bag squeeze.

RMS: root-mean-squared average of flow in the plateau of the flow rate profile.

Q_{90}: Flow rate below which 90% of all measured values occur.

Table 3

The effect of orifice size (3.6 mm) and capsule piercing Cases 1–3 on the mean AS device retention and aerosolization behavior at the exit of the ECG cannula actuating the 1 liter bag four times through the 3.6–565-ECG device. The DPI was connected to the streamlined ECG cannula through a 13 cm long tube (10 mm diameter) and the particle sizing was obtained using the NGI. The standard deviation (SD) is shown in parenthesis [n=3].

Description	Case 1	Case 2	Case 3
ED (%)	51.6 (13.3)	69.0 (0.6)	55.6 (5.7)
Capsule (%)	26.1 (15.9)	7.8 (0.1)	19.5 (8.5)
CC (%)*	3.1 (0.4)	0.7 (0.1)**	3.4 (1.1)
Flow passage (%)	7.1 (2.0)	8.4 (0.3)	9.7 (1.7)
Connecting tubing (13 cm) (%)	10.1 (0.7)	11.5 (0.3)	9.8 (3.0)
ECG Cannula (%)	1.9 (0.3)	2.5 (0.2)	1.9 (0.5)
$FPF_{<5\mu m/ED}$ (%)	80.0 (7.3)	73.2 (6.0)	82.9 (1.7)
$FPF_{<1\mu m/ED}$ (%)*	23.8 (2.8)	19.5 (3.1)	27.4 (3.0)
MMAD (μm)	1.89 (0.24)	2.20 (0.26)	1.71 (0.09)

*$P<0.05$ significant effect of piercing configuration on % CC drug retention and $FPF_{<1\mu m/ED}$ (one-way ANOVA).

**P<0.05 significant effect compared to Case 1 (post-hoc Tukey).

Table 4

The effect of number of bag actuations on emptying and AS deaggregation with the 3.1–565-ECG device using Case 3 piercing [n=3; Mean(SD)]. The data for four actuations is repeated from Table 1 for comparison.

Description	Two actuations	Four actuations
ED (%)	72.1 (2.5)	71.1 (1.0)
$FPF_{<5\mu m/ED}$ (%)	77.6 (8.3)	83.1 (1.4)
$FPF_{<1\mu m/ED}$ (%)	26.1 (5.4)	30.3 (1.6)
MMAD (μm)	1.48 (0.11)	1.39 (0.05)

Table 5

The effect of coating the device and capsule with PTFE on the mean AS emitted dose and aerosolization performance for the 3.1–565-ECG device using Case 3 piercing with two bag actuations [n=3; Mean(SD)]. The data for two actuations without PTFE is repeated from Table 4 for comparison.

Description	No PTFE	PTFE
ED (%)	72.1 (2.5)	78.2 (0.9)*
$FPF_{<5\mu m/ED}$ (%)	77.6 (8.3)	78.9 (5.8)
$FPF_{<1\mu m/ED}$ (%)	26.1 (5.4)	25.8 (3.8)
MMAD (μm)	1.48 (0.11)	1.47 (0.07)

* $p<0.05$ significant difference between no PTFE and PTFE coating for ED (independent samples t-test).

Table 6

Comparison between the mean AS emitted dose and aerosolization performance for the 3.1–565-ECG and CC_{90}-3D devices (four bag actuations). The data for the 3.1–565-ECG device is repeated from Table 1 for comparison.

Description	3.1–565-ECG	CC_{90}-ECG
ED (%)	71.1 (1.0)	66.4 (2.2)*
$FPF_{<5\mu m/ED}$ (%)	83.1 (1.4)	85.6 (0.7)*
$FPF_{<1\mu m/ED}$ (%)	30.3 (1.6)	30.9 (0.6)
MMAD (μm)	1.39 (0.05)	1.42 (0.01)

* $p<0.05$ significant difference between the devices for ED and $FPF_{<5\mu m/ED}$ (independent samples t-test).

Table 7

Flow profiles for the 2.3–343-ECG and 2.3–212-ECG devices based on total average flow, RMS, and Q_{90} metrics [n≥3; mean (SD)]. The maximum instantaneous flow rate recorded is also reported.

Method	2.3–343-ECG			2.3–212-ECG		
	Flow rate (LPM)	**Duration (s)**	**Maximum flow (LPM)**	**Flow rate (LPM)**	**Duration (s)**	**Maximum flow (LPM)**
Total average	10.8 (1.2)	3.4 (0.6)	21.6 (0.7)	8.0 (0.9)	3.5 (0.8)	14.0 (0.6)
RMS	14.7 (0.9)	2.0 (0.3)		11.6 (0.6)	1.5 (0.3)	
Q_{90}	18.1 (1.1)	3.4 (0.6)		13.1 (0.6)	3.5 (0.8)	

Total average: Average of all flow values for entire bag squeeze.

RMS: root-mean-squared average of flow in the plateau of the flow rate profile.

Q_{90}: Flow rate below which 90% of all measured values occur.

Table 8

The effect of orifice size (3.1 vs. 2.3 mm) and 3D rod configuration on the mean AS emitted dose and aerosolization performance with four bag actuations. The data for the 3.1–565-ECG device is taken from Table 1 for comparison.

Description	3.1–565-ECG	2.3–343-ECG	2.3–212-ECG
ED (%)	71.1 (1.0)	75.3 (2.5)	68.8 (4.4)
$FPF_{<5\mu m/ED}$ (%)*	83.1 (1.4)	65.4 (6.4)**	60.2 (8.5)**
$FPF_{<1\mu m/ED}$ (%)*	30.3 (1.6)	20.7 (3.0)**	21.1 (4.7)**
MMAD (μm)*	1.39 (0.05)	1.64 (0.07)**	1.59 (0.07)**

* $P<0.05$ significant effect of device on % $FPF_{<5\mu m/ED}$, $FPF_{<1\mu m/ED}$ and MMAD (one-way ANOVA).

** $P<0.05$ significant differences compared to 3.1–565-ECG (post-hoc Tukey).